Isomeric Excitation Energy for $^{99}In^{m}$ from Mass Spectrometry Reveals Constant Trend Next to Doubly Magic ^{100}Sn

L. Nies,[1,2,*] D. Atanasov,[1,†] M. Athanasakis-Kaklamanakis,[1,3] M. Au,[1,4] K. Blaum,[5] J. Dobaczewski,[6,7] B. S. Hu,[8] J. D. Holt,[8,9] J. Karthein,[10] I. Kulikov,[11] Yu. A. Litvinov,[11,12] D. Lunney,[13] V. Manea,[13] T. Miyagi,[14,12,5] M. Mougeot,[1,5,‡] L. Schweikhard,[2] A. Schwenk,[14,12,5] K. Sieja,[15] and F. Wienholtz[14]

[1]*European Organization for Nuclear Research (CERN), 1211 Geneva 23, Switzerland*
[2]*Institut für Physik, Universität Greifswald, 17487 Greifswald, Germany*
[3]*KU Leuven, Instituut voor Kern- en Stralingsfysica, B-3001 Leuven, Belgium*
[4]*Johannes Gutenberg-Universität Mainz, 55128 Mainz, Germany*
[5]*Max-Planck-Institut für Kernphysik, 69117 Heidelberg, Germany*
[6]*School of Physics, Engineering and Technology, University of York, Heslington, York YO10 5DD, United Kingdom*
[7]*Institute of Theoretical Physics, Faculty of Physics, University of Warsaw, Warsaw, ul. Pasteura 5, PL-02-093 Warsaw, Poland*
[8]*TRIUMF, TRIUMF 4004 Wesbrook Mall, Vancouver, British Columbia V6T 2A3, Canada*
[9]*Department of Physics, McGill University, Montréal, Quebec H3A 2T8, Canada*
[10]*Massachusetts Institute of Technology, Cambridge, Massachusetts 02139, USA*
[11]*GSI Helmholtzzentrum für Schwerionenforschung GmbH, 64291 Darmstadt, Germany*
[12]*ExtreMe Matter Institute EMMI, GSI Helmholtzzentrum für Schwerionenforschung GmbH, 64291 Darmstadt, Germany*
[13]*Université Paris-Saclay, CNRS/IN2P3, IJCLab, 91405 Orsay, France*
[14]*Institut für Kernphysik, Technische Universität Darmstadt, 64289 Darmstadt, Germany*
[15]*IPHC, CNRS/IN2P3 et Université de Strasbourg, F-67037 Strasbourg, France*

(Received 2 February 2023; revised 10 April 2023; accepted 2 June 2023; published 14 July 2023)

The excitation energy of the $1/2^-$ isomer in ^{99}In at $N = 50$ is measured to be 671(37) keV and the mass uncertainty of the $9/2^+$ ground state is significantly reduced using the ISOLTRAP mass spectrometer at ISOLDE/CERN. The measurements exploit a major improvement in the resolution of the multireflection time-of-flight mass spectrometer. The results reveal an intriguing constancy of the $1/2^-$ isomer excitation energies in neutron-deficient indium that persists down to the $N = 50$ shell closure, even when all neutrons are removed from the valence shell. This trend is used to test large-scale shell model, *ab initio*, and density functional theory calculations. The models have difficulties describing both the isomer excitation energies and ground-state electromagnetic moments along the indium chain.

DOI: 10.1103/PhysRevLett.131.022502

Considerable experimental and theoretical efforts have concentrated on the region around ^{100}Sn [1], the heaviest known self-conjugate and doubly magic nucleus ($N = Z = 50$), including decay spectroscopy [2–9], laser spectroscopy [10–12], Coulomb excitation studies [13–15], and mass measurements [16–19]. The similar valence orbitals that the protons and neutrons occupy are expected to enhance the effect of proton-neutron pairing, while the proximity of the double shell closure and proton drip line make it a unique laboratory to test our understanding of the strong interaction. However, core-excitation effects, i.e., the promotion of nucleons across shell gaps, can complicate the single- or few-particle picture even near shell closures, making accurate theoretical predictions difficult.

Theoretical approaches to calculate the properties of neutron-deficient nuclei near ^{100}Sn are computationally costly due to the large configuration space required. Nevertheless, the large-scale shell model (LSSM), the Monte Carlo shell model, and *ab initio* approaches have been successfully used in the tin region to describe, e.g., β-decay rates, quadrupole collectivity, and the enhanced magicity in ^{132}Sn [4,20–24].

In the indium isotopic chain, the single proton hole below the $Z = 50$ shell closure provides insight into the effective proton-neutron interaction. Mass measurements of the ground states in ^{99}In and ^{100}In were recently used to test *ab initio* calculations extended to a medium-mass odd-Z isotopic chain [18], thus providing valuable input for shell-model coupled-cluster (CCSM) calculations [25]. Moreover, recent results from laser spectroscopy revealed

the emergence of nuclear collectivity in neutron-rich indium isotopes, with the $9/2^+$ ground state abruptly departing the single-particle limit below $N = 82$ [10].

Nuclear isomers are particularly important for nuclear-structure studies [26] and their long lifetimes allow access to a broader range of experimental techniques. Measurements on the $N = 50$ isomer are an important milestone because they will reveal the effects of completely removing neutron excitations from the valence space, especially compared to $N = 82$. Its excitation energy will provide direct access to the energy difference between the configurations in which the proton hole occupies the $\pi g_{9/2}$ orbital (ground state) and $\pi p_{1/2}$ orbital (isomer).

In this Letter, we present measurements of the isomeric excitation energies in neutron-deficient indium isotopes, including the first determination of the excitation energy of $^{99}\mathrm{In}^m$ at the $N = 50$ shell closure. The experimental results are compared to state-of-the-art LSSM [27] and density functional theory (DFT) [28] calculations, as well as to *ab initio* calculations using the valence-space in-medium similarity renormalization group (VS-ISMRG) [29,30] and the CCSM method [31]. Advances in these methods are not only of interest for nuclear shell structure investigations but are also frequently used in metrology, atomic physics, and quantum chemistry [32–34].

The neutron-deficient indium isotopes were produced at the ISOLDE radioactive ion beam facility at CERN [35,36] by impinging a 1.4 GeV proton beam onto a thick lanthanum carbide target. Elements produced by fission, spallation, and fragmentation diffused out of the heated target into a hot tantalum tube, where they were ionized by the hot surface and through an element-selective two-step laser scheme provided by ISOLDE-RILIS [37]. The radioactive ion beam was then extracted at 30 keV, mass separated, and delivered to the ISOLTRAP experiment [38]. There it was cooled and bunched in a linear radio-frequency quadrupole cooler and buncher (RFQ-cb) [39]. The bunched beam was then sent at 3.2 keV to the multireflection time-of-flight mass spectrometer (MR-TOF MS) [40]. After capturing the bunches using the in-trap lift technique and storage of a few tens of milliseconds, the beam was ejected [41] and analyzed by single-ion counting with a time-of-flight detector. For calibration and optimization, $^{85}\mathrm{Rb}^+$ and $^{133}\mathrm{Cs}^+$ ions from an offline source were used.

The mass m of the ion of interest is extracted from its measured time of flight t, compared to two reference masses m_1 and m_2 with flight times t_1 and t_2, respectively, $\sqrt{m} = C_{\mathrm{TOF}}\Delta_{\mathrm{Ref}} + \Sigma_{\mathrm{Ref}}/2$, where $\Delta_{\mathrm{Ref}} = \sqrt{m_1} - \sqrt{m_2}$, $\Sigma_{\mathrm{Ref}} = \sqrt{m_1} + \sqrt{m_2}$, and $C_{\mathrm{TOF}} = (2t - t_1 - t_2)/[2(t_1 - t_2)]$ [42]. The excitation energy $E = [(\Delta t/t_0)^2 + 2\Delta t/t_0]m_0c^2$ of an isomeric state can be directly related to the TOF difference Δt with respect to its ground state of mass m_0 and TOF t_0, with c being the speed of light.

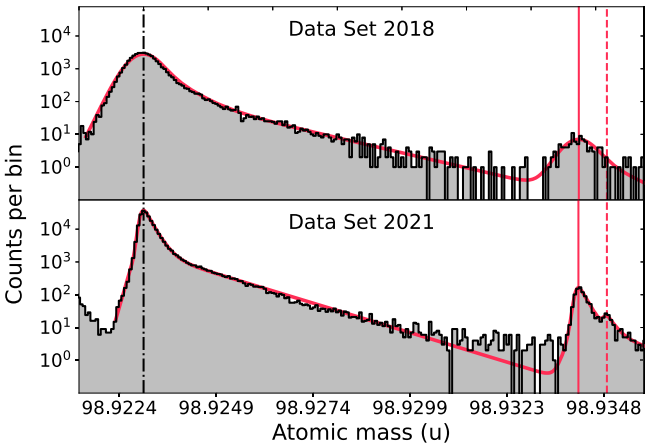

FIG. 1. Time-of-flight spectrum for the $m/q = 99$ beam in the MR-TOF MS with a hyperEMG fit [45] (red) to the data (see text for explanation). The top panel shows the 2018 dataset before the device improvements, and the lower panel shows the dataset from this Letter. The black (dash-dotted) line highlights the TOF for the strontium fluoride molecule. The vertical red lines show the ground state TOF (solid) and isomeric state TOF (dashed) of ^{99}In. The bin size is ~73 μu.

To achieve the resolving power $R = t_0/(2\Delta t_{\mathrm{FWHM}})$ necessary to separate the indium isomers, the capabilities of the MR-TOF MS were greatly enhanced. An extended active and passive multi-mirror voltage stabilization system based on Refs. [43,44] was implemented, which reduced Δt_{FWHM}. This not only allowed stable continuous operation of the device for more than 70 hours but also a much higher number of revolutions, between 1500 and 3000, increasing t_0. Furthermore, the initial ion-bunch emittance was optimized by synchronizing the experimental cycle to the 50-Hz AC power line and by fine-tuning the RFQ-cb ejection with respect to its radio-frequency field.

Figure 1 shows the TOF spectrum for the ISOLDE beam with mass-to-charge ratio $m/q = 99$ compared with the dataset from Ref. [18] to highlight the performance improvement. Surface-ionized contamination (here $^{80}\mathrm{Sr}^{19}\mathrm{F}^+$) was identified by calculating its mass m from its observed flight time t and comparing it to the known values of potential isotopes and molecules in the mass region. Indium was identified by its TOF and RILIS laser on-off tests. With an average proton current of 2.0 μA and about 3×10^{13} protons per pulse, roughly four $^{99}\mathrm{In}^+$ ions per second were extracted from the target on average. The ground-state-to-isomer ratio was determined to be 13∶1, resulting in less than 0.3 isomers per second delivered to the spectrometer.

TOF drifts were eliminated by calculating time-rolling averages of the reference SrF^+ molecule, thus quantifying the drifts and allowing to correct the TOF spectrum during the experiment, similar to Ref. [46]. For the TOF of 50 ms thus obtained for the indium ions, the resulting TOF widths of $\Delta t_{\mathrm{FWHM}} \approx 50$ ns allowed a mass resolving power of

TABLE I. Mass-measurement results for the indium isotopes given as C_{TOF} values (with mass excess calculated) for the ground states and as TOF difference Δt to the reference mass (with excitation energy calculated) for the isomeric states. Spin assignments J^{π}, half-lives, and reference masses are taken from the AME2020 [48] while the literature values marked with an asterisk are taken from Mougeot *et al.* [18]. Values marked with # are extrapolated or assigned from systematics. The uncertainties given for the mass excesses and the excitation energies correspond to statistical, followed by systematic uncertainties.

					Mass excess or exc. energy (keV)	
A	J^{π}	Half-life	Ref. ions	C_{TOF} or Δt (ns)	This Letter	Literature
99	$9/2^{+}$#	3.11(6) s	$^{80}Sr^{19}F^{+}$, $^{133}Cs^{+}$	$0.499\,646\,429(355)_{stat}(270)_{syst}$	$-61\,431(12)_{stat}(8)_{syst}$	$-61\,429(77)^{*}$
	$1/2^{-}$#	1 s#	$^{99gs}In^{+}$	$174(9)_{stat}(4)_{syst}$	$671(33)_{stat}(16)_{syst}$	400#(150#)
100	6^{+}#	5.62(6) s	$^{81}Sr^{19}F^{+}$, $^{85}Rb^{+}$	$0.499\,690\,777(350)_{stat}(156)_{syst}$	$-64\,191(11)_{stat}(5)_{syst}$	$-64\,178.1(22)^{*}$
101	$9/2^{+}$#	15.1(11) s	$^{82}Sr^{19}F^{+}$, $^{133}Cs^{+}$	$0.499\,677\,661(69)_{stat}(99)_{syst}$	$-68\,552.6(93)_{stat}(28)_{syst}$	$-68\,545.4(47)^{*}$
	$1/2^{-}$#	10 s#	$^{101gs}In^{+}$	$169.3(35)_{stat}(17)_{syst}$	$658(14)_{stat}(7)_{syst}$	$668(10.8)^{*}$

5×10^5, an improvement factor of 2.5 compared to our previous experiment [18]. The improvement helps not only the direct measurement of nuclear isomers and the isobaric purification for Penning-trap measurements but also increases long-term operation stability.

To extract the ground-state C_{TOF} value and the excitation energy of the isomeric state, a simultaneous fit of $^{80}Sr^{19}F^{+}$ and both $^{99}In^{+}$ states was performed. Because of the asymmetric nature of the TOF distribution, a multi-component exponentially modified Gaussian probability density function ("hyperEMG") [45] was used. This approach captures most of the tailing towards longer TOF, while small deviations from the model in the tail showed no influence on the mean of the Gaussian contribution to the fit, i.e., the extracted absolute TOF values.

To study systematic effects on the data evaluation method, radioactive ion beams were taken for $99 \leq m/q \leq 101$. The results are listed in Table I. The contaminant SrF^{+} served as the first reference to determine the C_{TOF} values, while $^{133}Cs^{+}$ from an offline ion source was used as the second reference. The relative production rates of the two indium states were similar along the investigated chain, suggesting, in combination with laser spectroscopy data [47], a $9/2^{+}$ and $1/2^{-}$ spin assignment to the ground and isomeric states, respectively. This is furthermore supported by a recent gamma-spectroscopy experiment of ^{99}In [9], which assigns spin $9/2^{+}$ to the dominantly produced state. The mass measurement results are in excellent agreement with previous studies [16–19], improving the precision of our former ^{99}In ground-state mass measurement by a factor of 5. Notably, the enhanced MR-TOF MS now achieved a similar precision as the Penning-trap experiment from [18].

In the simplest shell-model picture the ground and isomeric states are formed by a proton hole in the $\pi g_{9/2}$ and the $\pi p_{1/2}$ shells, respectively, determining the spins and parities of the two states. The evolution of their binding energies with neutron number, presented in Fig. 2, is influenced by the filling of the $\nu d_{5/2}$ and $\nu g_{7/2}$ neutron shells. The $Z = 50$ shell gap is formed between the $9/2^{+}$ states in indium and the $5/2^{+}$ states in antimony, also shown in Fig. 2. The present measurements extend the data down to $N = 50$. Although the experimental binding energies of the two states are not linear with neutron number, the splitting between the two states is almost constant (including that of ^{99}In, determined in this work to be about 670 keV), only changing at the $N = 64$ subshell closure. This is intriguing, considering the large variation in neutron number between $N = 50$ and $N = 64$.

To investigate the origin of this constant trend, we performed LSSM calculations with the effective interaction above a ^{88}Sr core employed previously to obtain β-decay half-lives around $N = 82$ [49,50]. To study neutron-deficient indium isotopes, the single-particle energies were adjusted to reproduce the spectrum of ^{91}Zr, while the $V_{g_{9/2}-g_{7/2}}$ $T = 0$ proton-neutron monopole interaction was made more attractive (by −600 keV) to match the observed shell evolution between ^{91}Zr and ^{101}Sn. The calculations

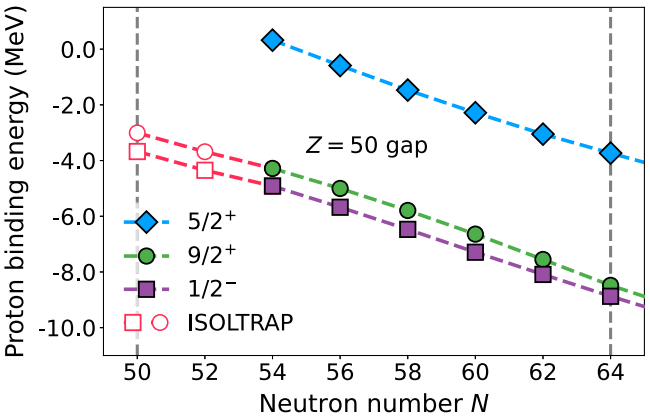

FIG. 2. Proton binding energies for nuclear states of the indium ($Z = 49$, green and purple) and antimony ($Z = 51$, blue) isotopic chains. Data taken from Ref. [48] (solid symbols) and this work (open symbols, red). The vertical dashed lines indicate the spherical shell closure at $N = 50$ and the subshell closure at $N = 64$.

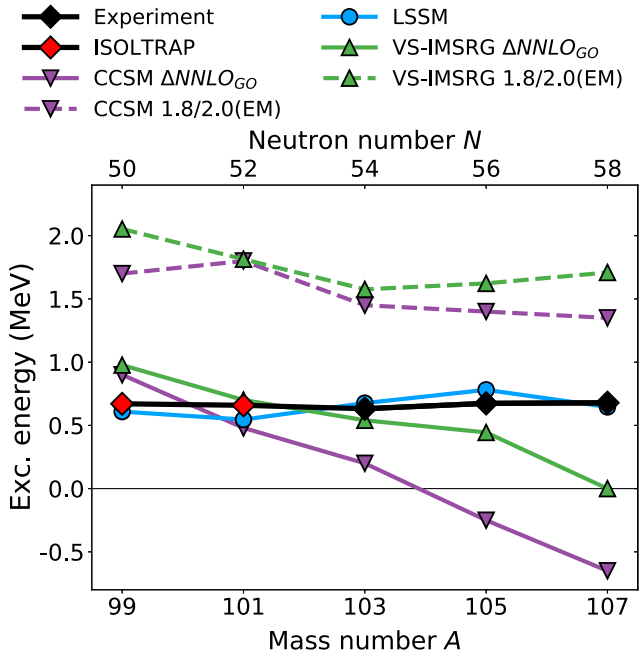

FIG. 3. Excitation energies for the $1/2^-$ states in odd-even neutron-deficient indium isotopes compared to large-scale shell model and *ab initio* calculations. The CCSM results are taken from [25].

were performed using the Strasbourg shell-model codes Antoine and NATHAN [27,51], maximally allowing for 4-particle–4-hole excitations for both neutrons and protons across the $N = Z = 50$ gap (3-particle–3-hole for $A = 105$, 107). The excitation energies are converged within 50 keV in all nuclei. The resulting energy splitting, shown in blue in Fig. 3, is very close to the experimental results.

The LSSM predicts states with very similar proton orbital occupation across the indium chain. The neutrons above $N = 50$ are located predominantly in the $\nu d_{5/2}$ and $\nu g_{7/2}$ orbitals, having little effect on the proton occupancy. The results indicate that the attractive monopole interaction between the $\pi g_{9/2}$ and the $\nu g_{7/2}$ nucleons is roughly compensated by the sum of the likewise attractive $T = 0$ $\pi p_{1/2} - \nu d_{5/2}$ and $\pi p_{1/2} - \nu g_{7/2}$ monopoles, which is likely the reason for the similar energy splittings of the two states. The slight variations of the $1/2^-$ energy may further relate to modifications of the relative population of neutron orbitals along the isotopic chain. This complex picture makes the excitation energy of the $1/2^-$ isomeric state an interesting benchmark for *ab initio* methods, which have only recently been applied to this region [18,22,25].

Thus, we present *ab initio* calculations using the VS-IMSRG and also compare to the CCSM results of Ref. [25], using the 1.8/2.0(EM) [52,53] and ΔNNLO$_{GO}$ interactions [54]. The VS-IMSRG calculations are performed in a 15 major-shell harmonic oscillator (HO) space. For the three-nucleon matrix elements, an additional $E_{3\,\mathrm{max}}$ truncation is required, defined as the sum of three-body HO principal quantum numbers. Here we use $E_{3\,\mathrm{max}} = 24$ which is sufficiently large in the $A \sim 100$ region [55] to achieve converged results. To explicitly capture the effect of excitations across the $N = Z = 50$ gap, both the proton and neutron $1p_{1/2}$, $1p_{3/2}$, $1d_{5/2}$, $0g_{7/2}$, and $0g_{9/2}$ spaces were decoupled above a ^{88}Se core using the multishell approach of Ref. [56]. While the full valence-space diagonalization is impossible, up to 5-particle–5-hole excitations across the $N = Z = 50$ gap were included. We observed that the excitation energies are converged to ≈70 keV with respect to the particle-hole truncation.

As shown in Fig. 3, the two employed interactions result in similar energy-splitting trends for both the VS-IMSRG and CCSM methods. The ΔNNLO$_{GO}$ interaction tends to be more accurate at the expense of a linear decrease of excitation energy with N leading to an inversion, which is at odds with the data. On the other hand, the 1.8/2.0(EM) interaction reproduces the rather flat trend of the splitting better and does not result in any state inversion, but overpredicts the magnitude of the splitting.

The state crossing in ^{107}In from the calculations with ΔNNLO$_{GO}$ can be understood by comparing the diagonal monopole matrix elements of the ΔNNLO$_{GO}$ and 1.8/2.0 (EM) valence-space interactions. Similar to what is found in the LSSM calculations, the flatness of the excitation energies for the 1.8/2.0 (EM) interaction results from the relevant monopole matrix elements and the balanced occupancy of $\nu g_{7/2}$ and $\nu d_{5/2}$. This similarity is reinforced by the observation that both interactions reproduce the energy splitting $\nu g_{7/2} - \nu d_{5/2}$ of the single-neutron state in ^{101}Sn [57] within 100 keV. Although the relevant matrix elements are almost the same for 1.8/2.0 (EM) and ΔNNLO$_{GO}$, the weaker $\nu p_{3/2} - \nu g_{7/2}$ monopole repulsion of the latter reduces the mixing between $\nu g_{7/2}$ and $\nu d_{5/2}$, leading to a larger $\nu g_{7/2} - \nu d_{5/2}$ splitting. In this case, the filled $\nu g_{7/2}$ configuration leads to a linear decrease.

For a broader view, in Fig. 4 we show the energy splitting across the full indium chain with recent nuclear moment measurements from Ref. [10], compared to theoretical calculations. (Note that for Ref. [10], the VS-IMSRG calculations were performed in a different valence space than the results shown in Fig. 3, leading to a slightly different energy splitting for $A \leq 107$.) In addition, we extend the DFT calculations of Ref. [10] to $N = 50$. Those were performed within the Hartree-Fock approximation for both protons and neutrons and thus they stagger with N owing to occupying consecutive individual single-particle deformed neutron orbitals. The complementary data show another remarkable constancy: that of the magnetic dipole moments of the $9/2^+$ ground state which are significantly lower than those expected in the single-particle configuration (the so-called Schmidt limit [58]), except for the value at the $N = 82$ closed shell. The excitation energy at $N = 82$, similar to $N = 50$, stays rather constant. From the VS-IMSRG calculations, this can be explained by the

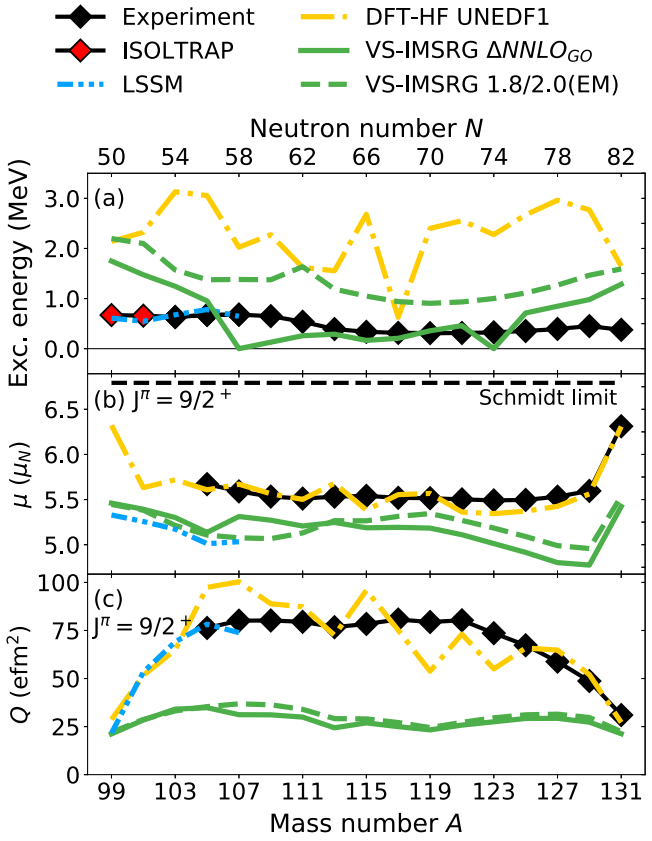

FIG. 4. Isomer excitation energies (a) and ground-state electromagnetic moments (b) and (c) of odd-even indium isotopes, compared to theoretical calculations. The experimental data are from [59] (black) and this work (red) for the excitation energies and from [10] for the moments. Both DFT-HF and VS-ISMRG calculations are from [10] and are extended in this work to reach $N = 50$.

monopole strengths, which are almost the same at $N = 50$ and $N = 82$, and are only weakly dependent on the number of neutrons.

While the differences between the excitation energy measurements and the DFT calculations are quite large for the density functional UNEDF1 [60] used here, a rather constant trend remains at the same level as the *ab initio* results [see Fig. 4(a)]. We note that in the DFT calculations, the isomer excitation energy is directly related to the strength of the spin-orbit interaction (see the discussion of the analogous excitation energy in silver isotopes [12]). Therefore, the measurements presented in this Letter provide an important anchor point for future global readjustments of nuclear density functionals.

By including time-odd fields, the DFT approach accurately reproduces the $9/2^+$ dipole moments μ. In contrast, the LSSM and VS-IMSRG calculations underestimate the absolute value but reproduce the general trend well [see Fig. 4(b)]. The sudden increase of the magnetic moment at $N = 82$ is well described by the DFT calculations, which predict a similar occurrence at $N = 50$. Intriguingly, the LSSM and *ab initio* calculations show a much smoother evolution towards $N = 50$. While the excitation energy is flat at $N = 82$ due to the cancellation of the monopoles in the VS-IMSRG calculations, the $9/2^+$ dipole moments are much more sensitive to the neutron configuration.

The DFT and LSSM calculations reproduce the quadrupole moments Q reasonably well, while the VS-IMSRG describes neither the absolute values nor the trend [see Fig. 4(c)]. This is most likely due to collective effects that are not fully captured when calculating the E2 matrix elements at the IMSRG(2) level [61].

In summary, the excitation energy of the $1/2^-$ isomer in ^{99}In has been measured for the first time, thanks to significant upgrades of the ISOLTRAP MR-TOF MS at ISOLDE/CERN. The systematics of the isomer excitation energy now reach the crucial $N = 50$ shell closure, confirming its constancy—even with no neutrons left in the valence shell. The shell model and the *ab initio* calculations using the 1.8/2.0(EM) interaction describe the constancy with the compensation of the monopole proton-neutron interactions, via a balanced occupation of the valence neutron orbitals. The ΔNNLO$_{GO}$ interaction results in a different occupation and leads to a linear decrease with neutron number, at odds with the experiment. Examining the electromagnetic moments of the $9/2^+$ ground states and including DFT calculations in the comparisons, we find that all models struggle to describe both energy and electromagnetic observables consistently. Measurements of nuclear moments of the $1/2^-$ and $9/2^+$ states down to $N = 50$ are needed to further benchmark the trends predicted by the calculations, as well as future theoretical developments.

We thank the ISOLDE technical group and the ISOLDE Collaboration for their support. We acknowledge the support of the German Max Planck Society, the French Institut National de Physique Nucléaire et de Physique des Particules (IN2P3), the European Research Council (ERC) under the European Union's Horizon 2020 research and innovation programme (Grant Agreements No. 682841 'ASTRUm', 654002 'ENSAR2', 101020842 'EUSTRONG', and 861198 'LISA'), as well as the German Federal Ministry of Education and Research (BMBF; Grants No. 05P18HGCIA, 05P21HGCI1, and 05P21RDFNB). L. N. acknowledges support from the Wolfgang Gentner Programme of the German Federal Ministry of Education and Research (Grant No. 13E18CHA). This work was partially supported by the STFC Grants No. ST/P003885/1 and No. ST/V001035/1, by the Polish National Science Centre under Contract No. 2018/31/B/ST2/02220, and by a Leverhulme Trust Research Project Grant. The VS-IMSRG computations were in part performed with an allocation of computing resources at the Jülich Supercomputing Center and with an allocation of computing resources on Cedar at WestGrid

and Compute Canada using imsrg++ [62] and KSHELL [63] codes. We acknowledge the CSC-IT Center for Science Ltd., Finland, for allocating computational resources. This project was partly undertaken on the Viking Cluster, which is a high-performance computing facility provided by the University of York. We are grateful for computational support from the University of York High Performance Computing service, Viking, and the Research Computing team. The experiment was conducted by M. A.-K., M. Au, D. A., K. B., I. K., Yu. A. L., D. L., V. M., M. M., L. N., and F. W. The theoretical calculations were performed by J. D., B. S. H., J. D. H, T. M., A. S., and K. S. All authors contributed to the preparation of the manuscript.

*Lukas.Nies@cern.ch
†Present address: LP2i Bordeaux, UMR5797, Université de Bordeaux, CNRS, France.
‡Present address: University of Jyväskylä, Department of Physics, Accelerator laboratory, P.O. Box 35(YFL), FI-40014, Finland.

[1] T. Faestermann, M. Górska, and H. Grawe, The structure of ^{100}Sn and neighbouring nuclei, Prog. Part. Nucl. Phys. **69**, 85 (2013).
[2] I. G. Darby, R. K. Grzywacz, J. C. Batchelder, C. R. Bingham, L. Cartegni, C. J. Gross, M. Hjorth-Jensen, D. T. Joss, S. N. Liddick, W. Nazarewicz, S. Padgett, R. D. Page, T. Papenbrock, M. M. Rajabali, J. Rotureau, and K. P. Rykaczewski, Orbital Dependent Nucleonic Pairing in the Lightest Known Isotopes of Tin, Phys. Rev. Lett. **105**, 162502 (2010).
[3] G. Lorusso *et al.*, β-delayed proton emission in the ^{100}Sn region, Phys. Rev. C **86**, 014313 (2012).
[4] C. B. Hinke *et al.*, Superallowed Gamow–Teller decay of the doubly magic nucleus ^{100}Sn, Nature (London) **486**, 341 (2012).
[5] J. Park *et al.*, β decays of the heaviest $N = Z - 1$ nuclei and proton instability of ^{97}In, Phys. Rev. C **97**, 051301 (2018).
[6] K. Auranen *et al.*, Superallowed α Decay to Doubly Magic ^{100}Sn, Phys. Rev. Lett. **121**, 182501 (2018).
[7] D. Lubos *et al.*, Improved Value for the Gamow-Teller Strength of the ^{100}Sn Beta Decay, Phys. Rev. Lett. **122**, 222502 (2019).
[8] J. Park *et al.*, New and comprehensive β- and βp-decay spectroscopy results in the vicinity of ^{100}Sn, Phys. Rev. C **99**, 034313 (2019).
[9] J. Park *et al.*, Spectroscopy of ^{99}Cd and ^{101}In from β decays of ^{99}In and ^{101}Sn, Phys. Rev. C **102**, 014304 (2020).
[10] A. R. Vernon *et al.*, Nuclear moments of indium isotopes reveal abrupt change at magic number 82, Nature (London) **607**, 260 (2022).
[11] X. Yang, S. Wang, S. Wilkins, and R. G. Ruiz, Laser spectroscopy for the study of exotic nuclei, Prog. Part. Nucl. Phys. **129**, 104005 (2023).
[12] R. de Groote *et al.*, Measurements of Binding Energies and Electromagnetic Moments of Silver Isotopes—A Complementary Benchmark of Density Functional Theory (to be published).
[13] C. Vaman *et al.*, $Z = 50$ Shell Gap near ^{100}Sn from Intermediate-Energy Coulomb Excitations in Even-Mass $^{106-112}$Sn Isotopes, Phys. Rev. Lett. **99**, 162501 (2007).
[14] V. M. Bader, A. Gade, D. Weisshaar, B. A. Brown, T. Baugher, D. Bazin, J. S. Berryman, A. Ekström, M. Hjorth-Jensen, S. R. Stroberg, W. B. Walters, K. Wimmer, and R. Winkler, Quadrupole collectivity in neutron-deficient Sn nuclei: ^{104}Sn and the role of proton excitations, Phys. Rev. C **88**, 051301(R) (2013).
[15] G. Guastalla *et al.*, Coulomb Excitation of ^{104}Sn and the Strength of the ^{100}Sn Shell Closure, Phys. Rev. Lett. **110**, 172501 (2013).
[16] X. Xu *et al.*, Masses of ground and isomeric states of ^{101}In and configuration-dependent shell evolution in odd-A indium isotopes, Phys. Rev. C **100**, 051303(R) (2019).
[17] C. Hornung *et al.*, Isomer studies in the vicinity of the doubly-magic nucleus ^{100}Sn: Observation of a new low-lying isomeric state in ^{97}Ag, Phys. Lett. B **802**, 135200 (2020).
[18] M. Mougeot *et al.*, Mass measurements of $^{99-101}$In challenge *ab initio* nuclear theory of the nuclide ^{100}Sn, Nat. Phys. **17**, 1099 (2021).
[19] Y. M. Xing *et al.*, Isochronous mass measurements of neutron-deficient nuclei from ^{112}Sn projectile fragmentation, Phys. Rev. C **107**, 014304 (2023).
[20] L. Coraggio, A. Covello, A. Gargano, N. Itaco, and T. T. S. Kuo, Shell-model study of quadrupole collectivity in light tin isotopes, Phys. Rev. C **91**, 041301(R) (2015).
[21] T. Togashi, Y. Tsunoda, T. Otsuka, N. Shimizu, and M. Honma, Novel Shape Evolution in Sn Isotopes from Magic Numbers 50 to 82, Phys. Rev. Lett. **121**, 062501 (2018).
[22] T. D. Morris, J. Simonis, S. R. Stroberg, C. Stumpf, G. Hagen, J. D. Holt, G. R. Jansen, T. Papenbrock, R. Roth, and A. Schwenk, Structure of the Lightest Tin Isotopes, Phys. Rev. Lett. **120**, 152503 (2018).
[23] P. Gysbers, G. Hagen, J. D. Holt, G. R. Jansen, T. D. Morris, P. Navrátil, T. Papenbrock, S. Quaglioni, A. Schwenk, S. R. Stroberg, and K. A. Wendt, Discrepancy between experimental and theoretical β-decay rates resolved from first principles, Nat. Phys. **15**, 428 (2019).
[24] A. P. Zuker, Quadrupole dominance in the light Sn and in the Cd isotopes, Phys. Rev. C **103**, 024322 (2021).
[25] Z. H. Sun, G. Hagen, G. R. Jansen, and T. Papenbrock, Effective shell-model interaction for nuclei "southeast" of ^{100}Sn, Phys. Rev. C **104**, 064310 (2021).
[26] A. Jain, B. Maheshwari, and A. Goel, *Nuclear Isomers: A Primer* (Springer International Publishing, New York, 2021).
[27] E. Caurier, G. Martínez-Pinedo, F. Nowacki, A. Poves, and A. P. Zuker, The shell model as a unified view of nuclear structure, Rev. Mod. Phys. **77**, 427 (2005).
[28] N. Schunck, ed., *Energy Density Functional Methods for Atomic Nuclei* (IOP Publishing, Bristol, 2019).
[29] S. R. Stroberg, A. Calci, H. Hergert, J. D. Holt, S. K. Bogner, R. Roth, and A. Schwenk, A Nucleus-Dependent Valence-Space Approach to Nuclear Structure, Phys. Rev. Lett. **118**, 032502 (2017).

[30] S. R. Stroberg, H. Hergert, S. K. Bogner, and J. D. Holt, Nonempirical interactions for the nuclear shell model: An update, Annu. Rev. Nucl. Part. Sci. **69**, 307 (2019).
[31] Z. H. Sun, T. D. Morris, G. Hagen, G. R. Jansen, and T. Papenbrock, Shell-model coupled-cluster method for open-shell nuclei, Phys. Rev. C **98**, 054320 (2018).
[32] S. Patra, M. Germann, J.-P. Karr, M. Haidar, L. Hilico, V. I. Korobov, F. M. J. Cozijn, K. S. E. Eikema, W. Ubachs, and J. C. J. Koelemeij, Proton-electron mass ratio from laser spectroscopy of HD^+ at the part-per-trillion level, Science **369**, 1238 (2020).
[33] R. X. Schüssler *et al.*, Detection of metastable electronic states by penning trap mass spectrometry, Nature (London) **581**, 42 (2020).
[34] R. J. Bartlett and M. Musiał, Coupled-cluster theory in quantum chemistry, Rev. Mod. Phys. **79**, 291 (2007).
[35] M. J. G. Borge and K. Blaum, Focus on exotic beams at ISOLDE: A laboratory portrait, J. Phys. G **45**, 010301 (2017).
[36] R. Catherall, W. Andreazza, M. Breitenfeldt, A. Dorsival, G. J. Focker, T. P. Gharsa, G. T. J, J.-L. Grenard, F. Locci, P. Martins, S. Marzari, J. Schipper, A. Shornikov, and T. Stora, The ISOLDE facility, J. Phys. G **44**, 094002 (2017).
[37] V. Fedosseev, K. Chrysalidis, T. D. Goodacre, B. Marsh, S. Rothe, C. Seiffert, and K. Wendt, Ion beam production and study of radioactive isotopes with the laser ion source at ISOLDE, J. Phys. G **44**, 084006 (2017).
[38] M. Mukherjee, D. Beck, K. Blaum, G. Bollen, J. Dilling, S. George, F. Herfurth, A. Herlert, A. Kellerbauer, H.-J. Kluge, S. Schwarz, L. Schweikhard, and C. Yazidjian, ISOLTRAP: An on-line Penning trap for mass spectrometry on short-lived nuclides, Eur. Phys. J. A **35**, 1 (2008).
[39] F. Herfurth, J. Dilling, A. Kellerbauer, G. Bollen, S. Henry, H.-J. Kluge, E. Lamour, D. Lunney, R. Moore, C. Scheidenberger, S. Schwarz, G. Sikler, and J. Szerypo, A linear radiofrequency ion trap for accumulation, bunching, and emittance improvement of radioactive ion beams, Nucl. Instrum. Methods Phys. Res., Sect. A **469**, 254 (2001).
[40] R. Wolf, F. Wienholtz, D. Atanasov, D. Beck, K. Blaum, C. Borgmann, F. Herfurth, M. Kowalska, S. Kreim, Y. A. Litvinov, D. Lunney, V. Manea, D. Neidherr, M. Rosenbusch, L. Schweikhard, J. Stanja, and K. Zuber, ISOLTRAP's multi-reflection time-of-flight mass separator/spectrometer, Int. J. Mass Spectrom. **349–350**, 123 (2013).
[41] F. Wienholtz, S. Kreim, M. Rosenbusch, L. Schweikhard, and R. Wolf, Mass-selective ion ejection from multi-reflection time-of-flight devices via a pulsed in-trap lift, Int. J. Mass Spectrom. **421**, 285 (2017).
[42] F. Wienholtz *et al.*, Masses of exotic calcium isotopes pin down nuclear forces, Nature (London) **498**, 346 (2013).
[43] F. Wienholtz, K. Blaum, J. Karthein, D. Lunney, S. Malbrunot-Ettenauer, V. Manea, M. Mougeot, L. Schweikhard, T. Steinsberger, and R. Wolf, Improved stability of multi-reflection time-of-flight mass spectrometers through passive and active voltage stabilization, Nucl. Instrum. Methods Phys. Res., Sect. B **463**, 348 (2020).
[44] P. Fischer and L. Schweikhard, Multiple active voltage stabilizations for multi-reflection time-of-flight mass spectrometry, Rev. Sci. Instrum. **92**, 063203 (2021).
[45] S. Purushothaman, S. Ayet San Andrés, J. Bergmann, T. Dickel, J. Ebert, H. Geissel, C. Hornung, W. Plaß, C. Rappold, C. Scheidenberger, Y. Tanaka, and M. Yavor, Hyper-EMG: A new probability distribution function composed of exponentially modified Gaussian distributions to analyze asymmetric peak shapes in high-resolution time-of-flight mass spectrometry, Int. J. Mass Spectrom. **421**, 245 (2017).
[46] P. Fischer, S. Knauer, G. Marx, and L. Schweikhard, Non-isobaric time-of-flight correction for isobar resolving in MR-ToF mass spectrometry, Int. J. Mass Spectrom. **432**, 44 (2018).
[47] J. Eberz, U. Dinger, G. Huber, H. Lochmann, R. Menges, R. Neugart, R. Kirchner, O. Klepper, T. Kühl, D. Marx, G. Ulm, and K. Wendt, Spins, moments and mean square charge radii of 104–127In determined by laser spectroscopy, Nucl. Phys. **A464**, 9 (1987).
[48] M. Wang, W. Huang, F. Kondev, G. Audi, and S. Naimi, The AME 2020 atomic mass evaluation (II). Tables, graphs and references, Chin. Phys. C **45**, 030003 (2021).
[49] F. Naqvi *et al.*, Isomer spectroscopy of ^{127}Cd, Phys. Rev. C **82**, 034323 (2010).
[50] Q. Zhi, E. Caurier, J. J. Cuenca-García, K. Langanke, G. Martínez-Pinedo, and K. Sieja, Shell-model half-lives including first-forbidden contributions for *r*-process waiting-point nuclei, Phys. Rev. C **87**, 025803 (2013).
[51] E. Caurier and F. Nowacki, Present status of shell model techniques, Acta Phys. Pol. B **30**, 705 (1999), https://www.actaphys.uj.edu.pl/R/30/3/705/pdf.
[52] K. Hebeler, S. K. Bogner, R. J. Furnstahl, A. Nogga, and A. Schwenk, Improved nuclear matter calculations from chiral low-momentum interactions, Phys. Rev. C **83**, 031301(R) (2011).
[53] J. Simonis, S. R. Stroberg, K. Hebeler, J. D. Holt, and A. Schwenk, Saturation with chiral interactions and consequences for finite nuclei, Phys. Rev. C **96**, 014303 (2017).
[54] W. G. Jiang, A. Ekström, C. Forssén, G. Hagen, G. R. Jansen, and T. Papenbrock, Accurate bulk properties of nuclei from $A = 2$ to ∞ from potentials with Δ isobars, Phys. Rev. C **102**, 054301 (2020).
[55] T. Miyagi, S. R. Stroberg, P. Navrátil, K. Hebeler, and J. D. Holt, Converged *ab initio* calculations of heavy nuclei, Phys. Rev. C **105**, 014302 (2022).
[56] T. Miyagi, S. R. Stroberg, J. D. Holt, and N. Shimizu, *Ab initio* multishell valence-space Hamiltonians and the island of inversion, Phys. Rev. C **102**, 034320 (2020).
[57] D. Seweryniak, M. P. Carpenter, S. Gros, A. A. Hecht, N. Hoteling, R. V. F. Janssens, T. L. Khoo, T. Lauritsen, C. J. Lister, G. Lotay, D. Peterson, A. P. Robinson, W. B. Walters, X. Wang, P. J. Woods, and S. Zhu, Single-Neutron States in ^{101}Sn, Phys. Rev. Lett. **99**, 022504 (2007).
[58] G. Neyens, Nuclear magnetic and quadrupole moments for nuclear structure research on exotic nuclei, Rep. Prog. Phys. **66**, 633 (2003).

[59] From ENSDF database as of January 26th, 2022. Version available at http://www.nndc.bnl.gov/ensarchivals/ (2022).
[60] M. Kortelainen, J. McDonnell, W. Nazarewicz, P.-G. Reinhard, J. Sarich, N. Schunck, M. V. Stoitsov, and S. M. Wild, Nuclear energy density optimization: Large deformations, Phys. Rev. C **85**, 024304 (2012).
[61] S. R. Stroberg, J. Henderson, G. Hackman, P. Ruotsalainen, G. Hagen, and J. D. Holt, Systematics of $E2$ strength in the *sd* shell with the valence-space in-medium similarity renormalization group, Phys. Rev. C **105**, 034333 (2022).
[62] S. R. Stroberg, https://github.com/ragnarstroberg/imsrg.
[63] N. Shimizu, T. Mizusaki, Y. Utsuno, and Y. Tsunoda, Thick-restart block Lanczos method for large-scale shell-model calculations, Comput. Phys. Commun. **244**, 372 (2019).